# GEOMAGNETIC VARIATIONS
# IN THE FREQUENCY RANGE 2.5–12 Hz IN THE IONOSPHERIC F LAYER
# AS MEASURED BY SWARM SATELLITES

**N.V. Yagova** (ID)
*Schmidt Institute of Physics of the Earth RAS,*
*Moscow, Russia, nyagova@ifz.ru*

**E.N. Fedorov** (ID)
*Schmidt Institute of Physics of the Earth RAS,*
*Moscow, Russia, enfedorov1@yandex.ru*

**V.A. Pilipenko** (ID)
*Schmidt Institute of Physics of the Earth RAS,*
*Moscow, Russia, pilipenko_va@mail.ru*
*Geophysical Center RAS,*
*Moscow, Russia*

**N.G. Mazur** (ID)
*Schmidt Institute of Physics of the Earth RAS,*
*Moscow, Russia, ngmazur@mail.ru*

**V.A. Martines-Bedenko** (ID)
*Schmidt Institute of Physics of the Earth RAS,*
*Moscow, Russia, lera_m0@mail.ru*

**Abstract.** We have analyzed geomagnetic variations in the 2.5–12 Hz frequency range in the ionospheric F layer above the electron density maximum, using data from two SWARM satellites. The analysis is based on the data obtained under weak and moderate magnetic activity for 12 days in September and December 2016. To separate spatial inhomogeneities from time variations, we analyzed signal waveforms and cross-spectra in a 2.56 s sliding window. A maximum in the occurrence and power spectral density of the variations was found at latitudes above the polar boundary of the auroral oval, which correspond to the magnetospheric input layers and dayside polar cusp/cleft. Typical waveforms of the high-latitude variations are the wave packets lasting for 5–10 periods, recorded with a short time delay by two satellites spaced by 40–100 km. These variations might be the ionospheric manifestation of the electromagnetic ion-cyclotron waves generated at the non-equatorial magnetosphere near the polar cusp. The waveforms and cross-spectra of the variations are examined in more details for two cases with different spatial distributions of the magnetic field in the ionosphere. For the ionospheric conditions corresponding to event 1 (September 17, 80° geomagnetic latitude, afternoon sector), spatial distributions of wave magnetic field in the ionosphere and on Earth are estimated using a model of Alfvén beam with a finite radius incident on the ionosphere [Fedorov et al., 2018].

**Keywords:** ionosphere, polar cusp, geomagnetic pulsations.

## INTRODUCTION

Magnetic field measurements with a 10–100 Hz sampling rate via low-orbit satellites have become available to a wide circle of researchers relatively recently. The region of hertz-range natural electromagnetic oscillations lies between geomagnetic pulsations and extremely low-frequency (ELF) radiation; properties of these oscillations in the ionosphere are still poorly studied. The frequency range from a few to tens of hertz corresponds to the highest harmonics of the ionospheric Alfvén resonator (IAR) [Polyakov, Rapoport, 1981; Belyaev et al., 1999]; and in the magnetosphere, depending on altitude, to the frequencies of ion-cyclotron and ion-ion hybrid (IIH) resonators [Buchsbaum, 1960]. The mechanisms of occurrence and propagation of ion-cyclotron and IIH waves in Earth's magnetosphere have been analyzed in the review [Mikhailova et al., 2022].

Another source of ionospheric oscillations in this frequency range is penetration of Schumann resonance harmonics into the ionosphere. Very few observations of penetration of the SHR harmonics into ionospheric heights have been published [Simões et al., 2011]. Simões et al. [2011] indicate the constant existence of electric field oscillations in the ionosphere at frequencies around 8 Hz, but no pronounced spectral maximum was observed at these frequencies in the magnetic field.

Due to the Doppler effect, the oscillations detected by low-orbit satellites may be a manifestation of lower-frequency small-scale oscillations [Le et al., 2011] or may result from the passage of a satellite through a quasi-static region of high magnetic field inhomogeneity, for example, when crossing the auroral oval. Multi-satellite measurements are required to correctly separate spatial inhomogeneities and time variations. This possibility arose after the launch of the ST5 [Slavin et al., 2008] and SWARM [Olsen et al., 2013] satellite missions. Three ST-5 satellites were set into quasi-meridian orbits. Distance between the satellites varied from 5000 to 50 km, which made it possible to separate temporal and spatial inhomogeneities on scales from ~10 s to 10 min.

The SWARM mission consists of three identical satellites: two at a distance of no more than 200 km from each other, and the third at a distance of several hundred

to several thousand kilometers from the first two satellites. This configuration makes up a space gradient system and allows us to study disturbances at different spatial scales. The ionospheric satellites are proving to be an effective tool for analyzing large-scale current structures, which is confirmed by simultaneous analysis of ionospheric and ground-based data [Juusola et al., 2016]. Lühr et al. [2015] have investigated the spatial structures of field-aligned currents in the auroral zone, using magnetic field measurement data from SWARM satellites, and have shown that the period during which changes in current structures with a spatial scale of 10 km may be neglected does not exceed 10 s. These studies were based on data with a sampling rate of 1 Hz. Geomagnetic pulsations of the Pc1 range (0.2–5 Hz) in the ionosphere as measured by ST-5 satellites have been studied in [Engebretson et al., 2008]. High-amplitude pulsations (>10 nT) were classified according to the number of satellites that recorded them. During three months of observations, 48 such events have been detected. Engebretson et al. [2008] have analyzed their distributions over frequencies of spectral maxima, $L$ shells, and local time. Over a third of the events were found in the outer magnetosphere ($L>9$), and frequencies of all the pulsations recorded in this region were below 1.5 mHz. Polarization and spatial scale of pulsations in the ionosphere and on Earth have been analyzed in [Pilipenko et al., 2012]. Oscillations in the ionosphere at altitudes 1000–4000 km were studied using magnetic field measurement data from ST-5 satellites. For mid-latitude Pc1 bursts recorded simultaneously by at least two satellites, the time delay between wave packets on the satellites was found to approximately correspond to the time determined from the distance between the satellites. This made it possible to estimate the spatial scale of the disturbances as several tens of kilometers.

In the outer magnetosphere, especially in the zones of maximum magnetic field gradients, as in the polar cusp, there are sharply anisotropic distributions of charged particles (such as oxygen of ionospheric origin), which effectively interact with ion-cyclotron waves [Le Queau, Roux, 1992]. Of particular significance for the oscillations of interest is a layer of the outer magnetosphere, such as the mantle, in which the ion flux is predominantly directed from the ionosphere. Comparative analysis of ion flux oscillations in the mantle region, as well as the magnetic field in the magnetosphere, as measured by the POLAR satellite, and in the cusp/cleft regions on the Earth surface [Engebretson et al., 2005] has shown that it is the mantle region that is the source of Pc1–2 (<1 Hz) waves propagating earthward. At the same time, there was no correspondence between frequencies of the oscillations and individual wave packets in the magnetosphere and on Earth. This is because the Pc1 waves do not propagate strictly along the magnetic field. For them there are waveguide propagation regions near Alfvén velocity minima in the magnetosphere [Leonovich et al., 1983] and in the ionosphere (see [Kim et al., 2011] and references therein). Kim et al. [2021] have studied ionospheric propagation of Pc1 pulsations ($f<5$ Hz), using SWARM measurements. The authors have

shown that the maximum occurrence of pulsations is observed at auroral latitudes, falling sharply as polar cap latitudes are approached.

Solar wind dynamic pressure jumps [Arnoldy et al., 2005] and magnetic impulse events observed as bursts lasting for about several minutes at the polar cusp/cleft latitudes [Lanzerotti et al., 1991; Kataoka et al., 2003] are considered as sources of Pc1 surface high-latitude waves. With sharp changes in the dynamic pressure, the proton temperature anisotropy increases and Pc1 pulsation bursts occur in the latitude range from the polar cap to the auroral oval [Arnoldy et al., 2005; Parkhomov et al., 2010]. The largest-scale Pc1 bursts are recorded from polar to midlatitudes and are associated with the arrival of the leading edge of an interplanetary shock wave even before the development of the main storm disturbance [Parkhomov et al., 2014]. Bursts of Pc1 pulsations at the latitudes of the dayside polar cusp are attributed to magnetic pulses [Sato et al., 1999]. Francia et al. [2020] deal with the Pc1 pulsations at frequencies below 1 Hz, which occur in two hemispheres from polar to auroral latitudes. In polar latitudes, in contrast to auroral ones, favorable conditions for generating the pulsations arise during weak and moderate disturbances. Under these conditions, the excitation of pulsations with close frequencies in a wide range of latitudes and ionospheric irregularities are observed simultaneously. At the polar cap latitudes, Pc1 pulsations occur as the so-called serpentine emission, i.e. quasi-regular pulsations with frequencies up to 5 Hz, whose occurance rate and amplitude are modulated with a period from a few to tens of minutes (see [Guglielmi et al., 2015] and references therein). They are likely to be related to electromagnetic ion-cyclotron (EMIC) waves in the interplanetary medium.

Magnetic field oscillations at frequencies above the nominal Pc1 range have been studied worse than Pc1 pulsations, and only a small number of publications are devoted to observations of these oscillations on Earth and in space. So, pulsations with frequencies to 15 Hz were detected at the mid-latitude station Novaya Zhyzn (McIlvain parameter $L=2.6$) during a magnetic storm in 2004 [Ermakova et al., 2015]. Calculations made by Ermakova et al. [2015] allow us to conclude that a source of these oscillations are ion-cyclotron waves excited at unusually low $L$ shells due to the equatorial displacement of the auroral oval during the storm.

The sources of the disturbances in a wide frequency range are the polar cusp and the boundary layers of the magnetosphere. The launch of the Cluster satellite mission consisting of four spacecraft, spaced several hundred to several thousand kilometers from each other, made it possible to study the spectral distributions of magnetic field variations in the cusp and in the magnetospheric input layers. Nykyri et al. [2006] have examined magnetic field variations and distributions of 10–40 keV ions when the Cluster satellites crossed the cusp at a distance of ~8 $R_E$ from the center of Earth. The oscillations had a power law spectrum with a constant slope from 1 to 8 Hz exhibiting up to five maxima corresponding, according to Nykyri et al. [2006], to the proton-cyclotron resonance harmonics. Jacobsen, Moen

[2010] have investigated electric field oscillations in the range from 1 to 100 Hz at intermediate altitudes in the cusp and their relationship with ion fluxes as measured by the Cluster-4 satellite. Significant positive correlations between ion fluxes and oscillation amplitude at averaging times of 30 and 60 s and the spectrum break at the local proton gyrofrequency, which was ~8 Hz for the events under study, argue for the local wave generation at intermediate altitudes in the cusp. Simultaneous study into electron and ion fluxes at medium distances from the equator in the cusp, cleft, and mantle, carried out in [Bogdanova et al., 2004] based on Cluster satellite measurements, has shown that an increase in the transverse temperature anisotropy of ions and the 1–10 Hz broadband electromagnetic emissions are associated with bursts of superthermal electron fluxes in the cleft region.

In this paper, we analyze geomagnetic variations in the frequency range from 2.5 to 12 Hz, which partially coincides with the nominal range of Pc1 pulsations, but also includes higher frequencies. The analysis is based on magnetic field measurement data from the SWARM-A and -C satellites. The satellites' orbits are quasi-meridional; the distance between the satellites varies from 40 km near the pole to 160 km at the equator. This allows us to separate disturbances of different spatial scales. In extreme cases, the oscillation frequencies recorded by the satellites may coincide with the frequency recorded by a stationary sensor, or may differ arbitrarily much from it. The former case is peculiar to wave disturbances whose spatial scale is much larger than the distance between the satellites; the latter corresponds to the passage of the satellite through quasi-static spatial inhomogeneities. In single-point observations, it is impossible to separate these cases, using measurements of the magnetic field alone. If measurements from two or more satellites are available, in the former case the maximum coherence will be observed with a time shift τ shorter than the oscillation period; and in the latter, with τ determined from the spatial scale of the wave disturbance structure and the satellite velocity. We deal with disturbances of the first type. Section 1 describes the measurement data and the processing method; Section 2 presents the results of data analysis; Sections 3 and 4 discuss the spatial structure of the Alfvén beam field of finite radius and the sources of the observed oscillations.

## 1.    DATA AND PROCESSING

Twelve days in September and December 2016 have been selected for the analysis. The selection criterion was the absence of magnetic storms with $Dst<-40$ nT during the whole day and four previous days. Auroral activity varied from weak to moderately high, and the minimum vertical component $B_z$ of the interplanetary magnetic field (IMF) for ten of the twelve days did not drop below –5 nT. Data on minimum and median $B_z$ and geomagnetic activity indices for 24 hours is given in Table.

The height of the satellites' orbits was around 450 km, i.e. above the maximum electron density. The measurement data on the three magnetic field components is available with a time resolution of 0.02 s. The analysis is based on the data after high-pass filtration with a cutoff frequency

of 1 Hz, which eliminates the effect of spatial variations in a constant field with a scale of the order of or larger than 10 km. We examine the time forms of oscillations of horizontal geomagnetic field components and their spectral parameters.

Magnetic field measurement data from SWARM satellites is available in the NEC (North-East-Center) satellite system oriented along geographic coordinates: the X component is oriented along the meridian; Z is directed to the center of Earth; and Y, to the east. For the high-latitude regions of interest, the angle between the main geomagnetic field and the vertical is small, i.e. the horizontal field components roughly correspond to the transverse ones. That said, the azimuth angle between the geographic and geomagnetic meridians at high latitudes can vary from 0 to 90°. Therefore, for each moment of time, using the adapted GEOPACK code [Papitashvili et al., 1997], we have recalculated the horizontal field components into a system oriented along corrected geomagnetic coordinates (CGM), where $B_N$ is the northward meridional field component, $B_E$ is the eastward latitudinal component. Since the model we employ does not allow calculations for the near-equatorial region, we analyze only the field variations for the geomagnetic latitudes above 27° in both hemispheres.

Cross-spectra were calculated by the Blackman—Tukey method in a window of 128 points (2.56 s) with smoothing by a 16-point Kaiser window [Jenkins, Watts, 1972]. The selected time window corresponds to a satellite passing a distance of ~20 km. For ~70 % of the intervals, the geomagnetic latitudes of the satellites at the same time point differ by more than 0.2° (22 km). We have chosen these intervals for the analysis because for them the difference in the time of passage of satellites over one geomagnetic latitude exceeds the length of the interval for which the spectrum is calculated, and several times exceeds the period of the oscillations under study.

From all the intervals for which we perform the spectral analysis, we have selected two groups for further study, determined from the power spectral density (*PSD*) at frequencies of local spectral maxima and spectral coherence of variations in the latitude component for the two satellites. We analyze the ratio of the total duration of the intervals for which *PSD* exceeds a given threshold to the total duration of all intervals, and the mean *PSD* value at the frequencies of spectral maxima. The threshold value of the spectral power density $PSD_b$ is set equal to $3 \cdot 10^{-5}$ nT$^2$/Hz, which corresponds to an oscillation amplitude of ~0.1 nT.

The same parameters are studied for the oscillations with the signal coherence in the two satellites above the threshold value of the coherence coefficient $\gamma_b^2 = 0.5$. Coherent intervals for which the difference between the geomagnetic latitudes of the satellites was small are excluded from consideration $\left(|\Delta\Phi| < 0.2^\circ\right)$ since in this case the similarity between the recorded signals can be caused by the simultaneous passage of the satellites through the structure stretched along the latitude. With such parameters, the high spectral coherence and the consistent change in the signal amplitude and frequency

Days under analysis and related magnetic activity parameters

| N | month/day | IMF $B_z$, nT | | $Dst$, nT | $AE$, nT | |
|---|---|---|---|---|---|---|
| | | min 24 hrs | median | min, 96 hrs | max, 24 hrs | median |
| 254 | 09/10 | –3.4 | –0.3 | –38 | 421 | 60 |
| 257 | 09/13 | –6.1 | –2.7 | –19 | 606 | 130 |
| 260 | 09/16 | –4.2 | 2.1 | –34 | 259 | 33 |
| 261 | 09/17 | –4.3 | 2.5 | –34 | 117 | 34 |
| 266 | 09/22 | –3.5 | 1.7 | –35 | 295 | 37 |
| 336 | 12/01 | –3.9 | 2.8 | –23 | 263 | 25 |
| 337 | 12/02 | –3.4 | –1.2 | –18 | 339 | 48 |
| 338 | 12/03 | –2.8 | –0.6 | –18 | 270 | 34 |
| 349 | 12/14 | –3.4 | 0.3 | –27 | 393 | 43 |
| 350 | 12/15 | –2.8 | 0.6 | –19 | 240 | 29 |
| 351 | 12/16 | 2.6 | 0.7 | –16 | 212 | 23 |
| 352 | 12/17 | –10.6 | 0.0 | –12 | 718 | 67 |
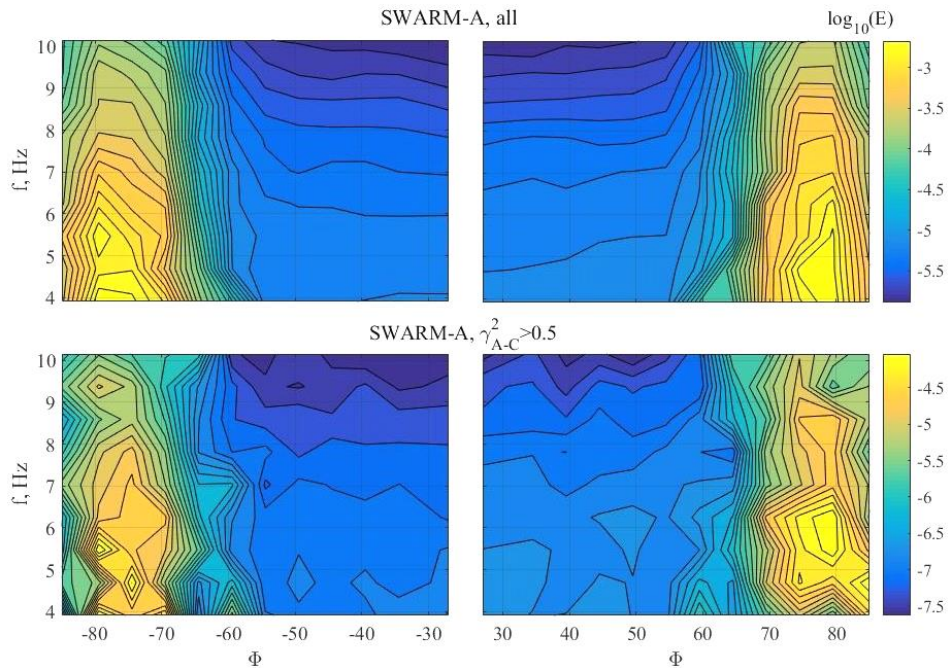


*Figure 1.* *PSD* distribution at frequencies of spectral maxima of variations in the magnetic field latitude component $B_E$ over geomagnetic latitude and frequency for all SWARM-A over-threshold oscillations (top panels) and those coherent to SWARM-A and -C oscillations (bottom panels) for the Southern (left) and Northern (right) hemispheres

in the time domain imply that the Doppler frequency shift is small and the signal frequency in the ionosphere is close to the frequency determined from satellite measurements.

The total length of the intervals such that $PSD>PSD_b$ is ~50 hrs. Hereinafter, we call these intervals over-threshold. The length of the intervals for which the conditions $\gamma^2 \geq 0.5$ and $|\Delta\Phi| > 0.2°$ hold is ~1.3 hrs. Further, they are termed as coherent and it is believed that the magnetic field variations recorded at that time can be considered as coherent oscillations observed simultaneously by two satellites.

## 2. RESULTS

### 2.1. Spatial distributions of spectral parameters

To localize sources of the ionospheric oscillations, let us figure out at which geomagnetic latitudes the over-threshold magnetic field variations and coherent oscilla-

tions in this frequency band generally occur, as well as how their occurrence is distributed over frequency.

Figure 1 illustrates the spatial distribution of *PSD* at the frequencies of spectral maxima of the latitude component $B_E$ for all SWARM-A over-threshold oscillations and those coherent at SWARM-A and SWARM-C. Along the X-axis is the corrected geomagnetic latitude $\Phi$; and along the Y-axis, the spectral maximum frequency $f$. For both types of signal, the maximum *PSD* value is observed at latitudes above 70° in both hemispheres. For the intervals with an arbitrary coherence value (top panels), the high-latitude maximum is seen at all frequencies, covering lower latitudes (up to 60°) at the low-frequency edge of the spectrum. For coherent intervals, we can identify specific maxima in the distribution. Thus, in the Southern (summer) Hemisphere, maxima are observed at frequencies of ~5.5 and 9.5 Hz at a latitude around –80° and at 4.5–5 Hz at –75°. In the Northern (winter) Hemisphere, wider maxima occur at 5–6 and 8–9 Hz at 75°–80°. Moreover, in both hemispheres at the low-frequency edge of the spectrum there

is a maximum at a latitude around 60° and small increases in *PSD* at frequencies below 7 Hz at lower latitudes. The presence of intervals with high signal coherence suggests that the observed magnetic field fluctuations are pulsations, and their frequencies are close to those recorded by the satellite. Let us next consider the regions of most intense variations corresponding to geomagnetic latitudes from 68° to 80° in both hemispheres.

Pin down how the occurrence and spectral power are distributed over geomagnetic latitudes Φ and local magnetic time (MLT). Figure 2 shows MLT distributions of a fraction *R* of the intervals of coherent oscillations and the PSD at spectral maximum frequencies for four latitudinal zones in the two hemispheres. For most of the day, *R* for all latitudinal zones varies between 0.02 and 0.04, and noticeable maxima of the occurrence of coherent oscillations are observed in the Southern Hemisphere at the highest latitudes in the morning (MLT=6) and afternoon (MLT=15) hours, with the afternoon maximum recorded in all latitudinal zones. In the Northern Hemisphere, the main maximum lies in the predawn sector (MLT=3) at latitudes 74°–77°.

During the daytime, *PSD* is significantly higher at higher latitudes (|Φ|>74°). This effect is most pronounced in the prenoon hours in both hemispheres when the difference between maximum and minimum *PSD* is as large as two orders of magnitude. The main difference in the *PSD* diurnal variation between the latitudinal zones |Φ|>74° in the Southern and Northern hemispheres is associated with higher values in the afternoon for 74°–77° in the Northern Hemisphere, where its values practically do not differ from those in the latitude range 77°–80°. In the Southern Hemisphere at 74°<|Φ|<77°, there is a weak minimum near noon, and

two maxima correspond to morning and afternoon hours. In the pre-midnight and midnight sectors, *PSD* in high-latitude zones decreases and its maximum shifts to auroral latitudes.

Thus, the main contribution to the high-latitude maxima in Figure 1 is made by the oscillation occurring during the daytime at geomagnetic latitudes from 74 to 80°. Magnetospheric projections of these regions are zones of the dayside polar cusp and input layers such as the mantle and the low-latitude boundary layer. The *PSD* values in the lowest latitudinal zone considered, which corresponds to the nominal auroral zone, are significantly lower. The decrease is also observed at high latitudes at night, i.e. near the polar caps. The maxima observed at the low-latitude edge of the region (|Φ|~60°) under study correspond to the Pc1 frequencies; and their position, to the plasmapause zone.

Estimates of the auroral oval position within the empirical model by Feldstein [1963] using the approximation by Holzworth, Meng [1975] of the auroral oval boundaries for the intervals of both over-threshold disturbances and coherent pulsations indicated that in fact in 75 % of cases coherent oscillations obtained by two satellites were detected above the auroral oval polar boundary. Thus, the oscillations considered generally occur near and above the auroral oval polar boundary; the auroral latitudes themselves feature noticeably lower oscillation amplitudes.

While the main spectral power of the oscillations is concentrated at frequencies below 6 Hz, local spectral maxima are regularly found at higher frequencies as well. Figure 3 shows probability density functions (PDF) of local spectral maximum frequencies for latitudinal zones above 71°. To ensure a sufficient number of cases for the analysis, the lower limit of the coherence
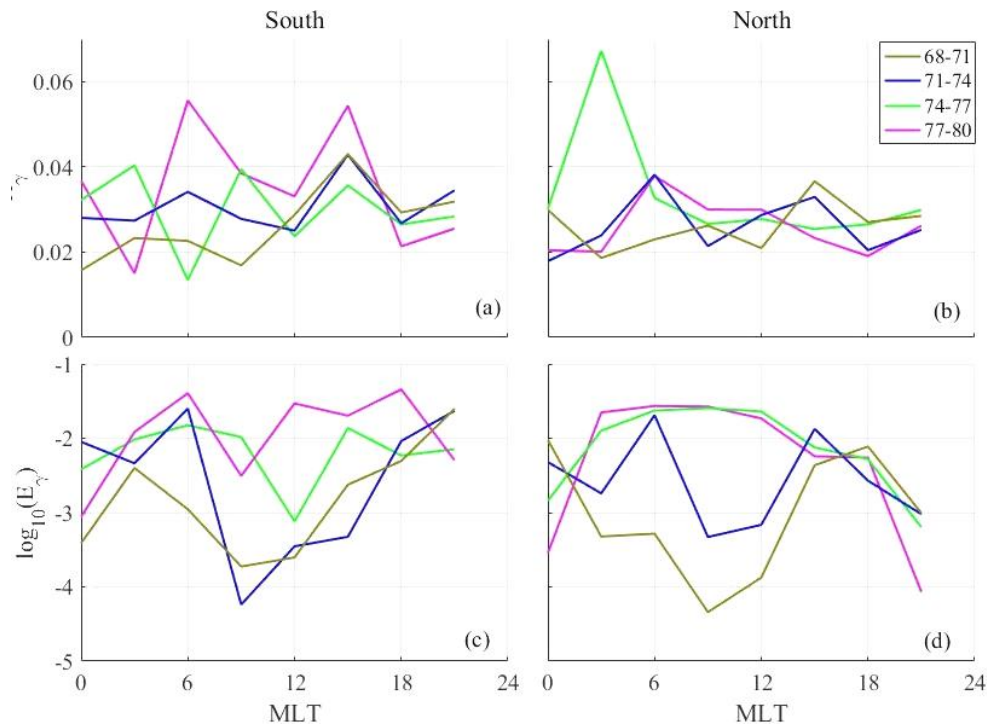


*Figure 2*. Occurrence rate (top panels) and spectral power (bottom panels) of coherent oscillations in four latitudinal zones for the Southern (left) and Northern (right) hemispheres
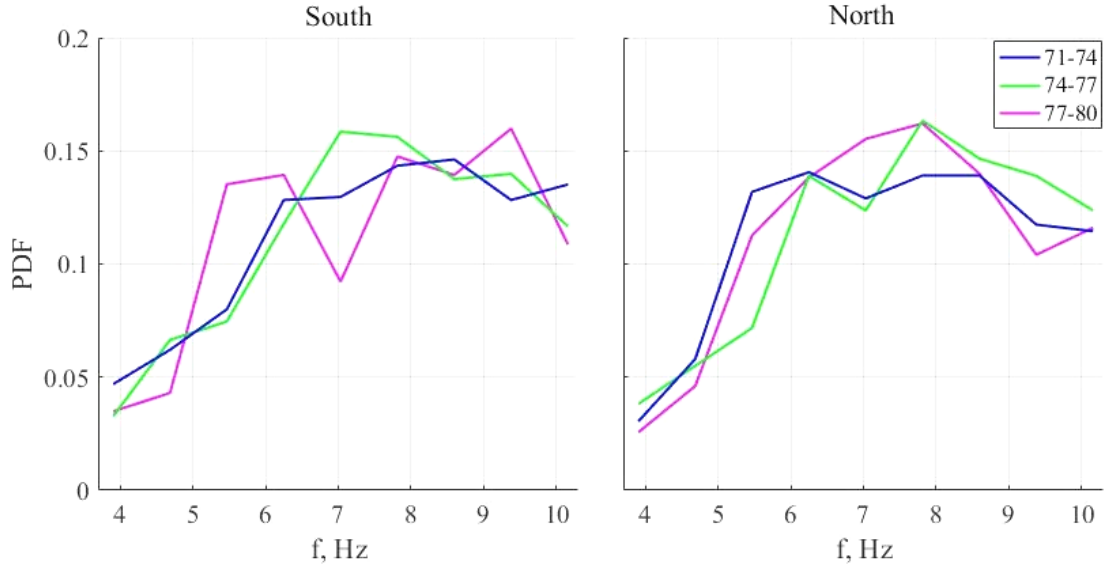
*Figure 3*. Empirical distribution functions (PDF) of frequencies of spectral maxima of coherent oscillations in three latitudinal zones for the Southern (left) and Northern (right) hemispheres

coefficient is set at $\gamma^2_{min} = 0.36$. In the Southern Hemisphere for the latitude zone 77°–80°, distribution maxima are at frequencies 5–6, 7.8, and 9.3 Hz. In the cusp zone 74°–77°, there is also a maximum at 9.3 Hz, and the highest maximum is observed in the frequency band 7–8 Hz. At 71°–74°, the distribution has the form of a wide dome with a maximum at 8.6 Hz. In the Northern Hemisphere, the distributions for all latitude intervals are shifted to lower frequencies with a main maximum at 7.8 Hz for two higher-latitude zones and two almost equal maxima at 6.3 and 8.6 Hz for 71°–74°.

Thus, the region of geomagnetic latitudes and MLT intervals corresponding to the dayside polar cusp and the magnetospheric input layers is the most favorable for the occurance of coherent magnetic field variations at frequencies of several hertz at distances of tens of kilometers in the ionosphere. The spectral maxima above 5 Hz, i.e. the upper boundary of the nominal range of Pc1 geomagnetic pulsations, are observed no less frequently than those below 5 Hz.

## 2.2. Analysis of individual events

Let us have a closer look at the signals in the time domain and the spectra of high-latitude oscillations obtained by the two satellites for separate intervals, here-inafter referred to as events 1 and 2. For event 1 (07:30:26 UT on September 17, 2016), intense oscillations were recorded at a geomagnetic latitude around 80° in the afternoon sector (MLT=15.9). The distance between the satellites was about 40 km, and the difference between geomagnetic latitudes was 0.35°, i.e. the satellites were located almost strictly along the magnetic meridian. According to the OVATION Prime model [Newell et al., 2002, 2010], at 7–8 UT the satellites' latitudes were slightly above the polar boundary of diffuse precipitation, and discrete precipitation was weak (Figure 4).

This position of the oval and the precipitation intensity fit the conditions of weak disturbance, as confirmed by the geomagnetic indices. The Dst index minimum for

four days (*Dst*=–34 nT) was detected two days before the event of interest — on September 15, which indicates a very weak magnetic storm whose recovery phase completely ended by the beginning of September 17 (*Dst*≥–2 nT). The auroral activity index *AE* was lower than 50 nT during the last five hours, i.e. there were no auroral disturbances during that period. Such conditions inside the magnetosphere were determined by parameters of the interplanetary medium with its long-term positive vertical component and minor solar wind dynamic pressure fluctuations near 2 nPa.

Figure 5 shows the waveforms and spectral parameters of variations in magnetic field horizontal components as observed by SWARM-A and -C. Both satellites observed oscillations with an amplitude of ~2 nT in the time interval 0–1 s, then a wave packet with a maximum amplitude of the latitude component $B_E$ appeared (the amplitude was as high as 10 nT according to SWARM-A
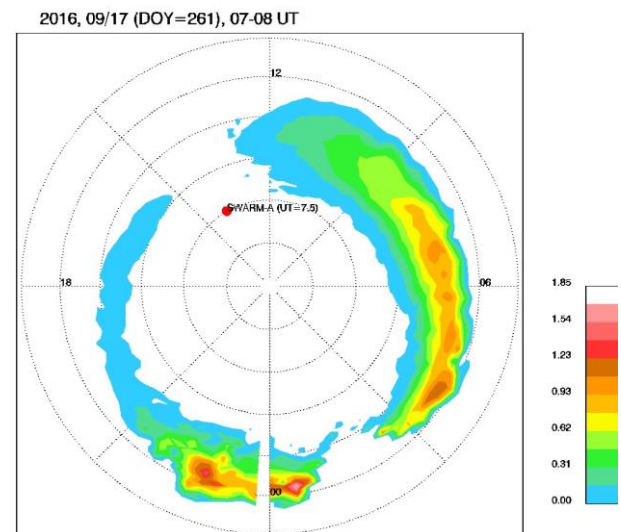


*Figure 4*. Diffuse precipitation intensity in the Northern Hemisphere for 07–08 UT on September 17, 2016 (day 261) as obtained by the OVATION Prime model
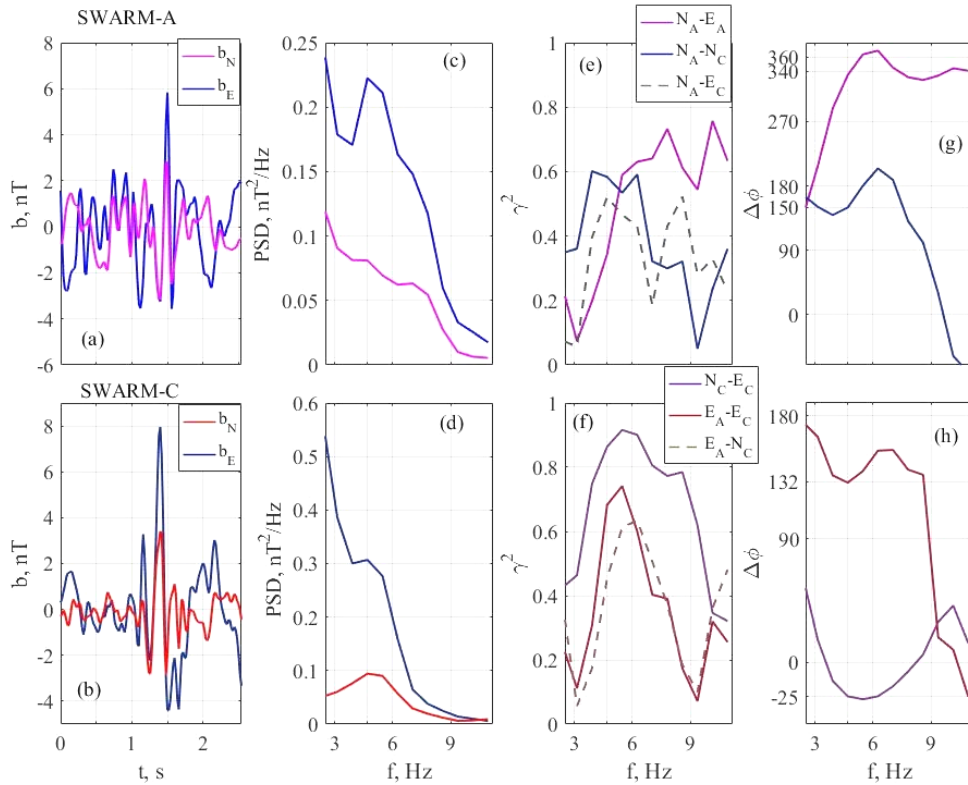
2016, DOY= 261, UT=07:30:26, $\Phi_1$= 79.65, $\Phi_2$= 80.00, MLT=15:54



*Figure 5*. Coherent oscillations recorded in the afternoon sector on September 17, 2016 (day 261, event 1). From left to right: time domain signal, *PSD* spectra, spectral coherence, and phase difference. Oscillations (*a, b*) and *PSD* spectra (*c, d*) for SWARM-A (top panels) and SWARM-C (bottom panels). For coherence spectra (*e, f*) and phase difference (*g, h*) the top panel shows cross-spectral parameters of the components according to the data from each satellite (SWARM-A (top panels) and SWARM-C (bottom panels)) and between the components according to the two satellites. The legend has the following structure: the letters N and E denote the meridional and latitudinal field components respectively, the index is a satellite, for example, $N_A$–$E_C$ corresponds to $B_N$ (SWARM-A) — $B_E$ (SWARM-C)

and 12 nT according to SWARM-C). The $B_E$ variations according to both satellites' data have maximum *PSD* at a frequency of ~4.7 Hz, and maximum *PSD* of $B_E$ is 0.22 nT$^2$/Hz (SWARM-A) and 0.3 nT$^2$/Hz (SWARM-C). The $B_N$ oscillation amplitudes are noticeably lower — in both satellites their maximum amplitude is ~5 nT. At 4.7 Hz, the $B_N$ *PSD* spectrum is maximum only in the case of SWARM-C; as for SWARM-A, this frequency exhibits a plateau. At this frequency, the spectral coherence $\gamma^2$ of the latitudinal and meridional components according to SWARM-C, as well as according to the two satellites, exceeds 0.5. Let us consider the phase differences at this particular frequency since both maximum *PSD* of the latitudinal component and a high coherence are observed at it. The phase difference between $B_E$ and $B_N$ for SWARM-A is –20° (340° in Figure 5, *g*) and –25° for SWARM-C; in both satellites, the ratio of *PSD* $B_E$ to *PSD* $B_N$ is about 3. At 4.7 Hz under high coherence, there are also maximum $B_E$ *PSD* variations, *PSD* of oscillations, recorded by the two satellites, differ less than 1.5 times, and the oscillations have almost the same polarization, as derived from the small differences in the *PSD* ratio to the phase difference between $B_E$ and $B_N$. The phase difference in $B_E$ according to the two satellites is 132°. Thus, the latitudinal com-

ponent variations in this event feature a significant phase change with a small change in amplitude at a distance between the satellites, and the amplitude increases with latitude. This suggests that the source of the oscillations in the ionosphere is located at a latitude intermediate between the geomagnetic latitudes of the satellites closer to SWARM-C.

In event 2 (18:18:26 UT on December 3, 2016), oscillations with an amplitude of several nT occurred at a geomagnetic latitude of ~78° in the pre-noon sector (MLT=10.66) under low geomagnetic activity. The *Dst* index did not decrease below –18 nT for previous four days, i.e. there was not even a weak magnetic storm. Current auroral activity was low (*AE*<50 nT), but two hours before the event there was a substorm with *AE*=140 nT. As in the previous event, there were no significant variations in the solar wind dynamic pressure, its absolute value fluctuated around 2 nPa, yet, unlike event 1, the IMF vertical component was negative: $B_z \approx -2$ nT.

Time forms and spectra of a signal are shown in Figure 6: signal distortions at a distance between the satellites are more significant than in event 1. The distance between the satellites was 75 km with ~0.5° difference between their geomagnetic latitudes, i.e. they were
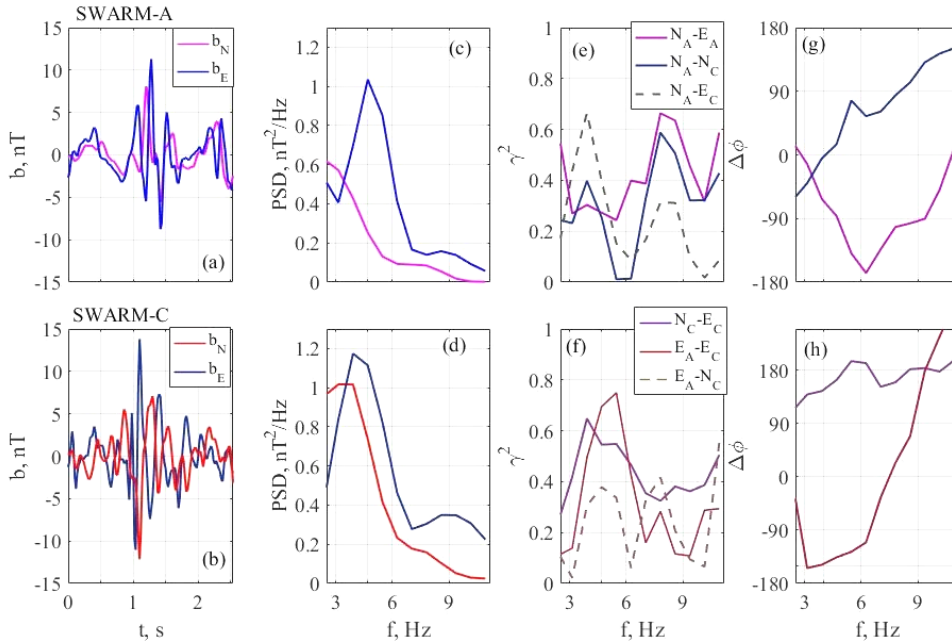
*Figure 6.* The same as in Figure 5 for coherent oscillations recorded in the pre-noon sector on December 3, 2016 (day 338, event 2)

spaced away by 55 km along the meridian. The signal amplitude was higher for SWARM-C, located closer to noon and at a higher latitude than SWARM-A. The maximum amplitude of $B_E$ was ~20 nT for both satellites, and $B_N$ was 18 nT for SWARM-C and 10 nT for SWARM-A. Meanwhile, the small shift in the time of onset of the disturbance and almost synchronous amplitude variations suggest a common origin of the signal.

The main spectral maximum of $B_E$ lies at a frequency of 4.7 Hz for SWARM-A and 4 Hz for SWARM-C. Moreover, in both cases an additional maximum in the spectra is seen at around 9 Hz. Nevertheless, only the main spectral maximum at 4.7 Hz falls into the region of high spectral coherence $\gamma^2 \approx 0.6$ of variations in $B_E$ and $B_N$ for SWARM-C and in latitudinal components for the two satellites. In the vicinity of the second maximum, the coherence of the latitudinal components turns out to be low. Thus, it makes sense to estimate the phase difference between $B_E$ variations for the two satellites only at the main spectral maximum frequency of 4.7 Hz. It is –150°. At the same frequency, the phase difference between the horizontal components for SWARM-C is 135°, which corresponds to elliptical polarization.

According to data from both satellites, the meridional component dominates at frequencies below 3.5 Hz; and the latitude component, above the frequencies; yet, for SWARM-A at $f > 3.5$ Hz the power ratio $B_N/B_E$ is significantly lower than for SWARM-C. For the meridional component in the case of SWARM-A, maximum *PSD* is observed at the left spectrum edge (2.7 Hz); and in the case of SWARM-C, at 4 Hz. In addition, in the meridional component spectra at around 7 Hz, there is a slowdown in the decrease (SWARM-C) and a plateau (SWARM-A). Coherence spectrum maxima are indicated as the maximum *PSD* spectrum frequency of 4 Hz at which $\gamma^2 \approx 0.4$, and as the 7.8 Hz frequency at which $\gamma^2 \approx 0.6$. The phase difference in $B_N$ at these frequencies is

about 0 and 90° respectively, i.e. it differs significantly at the frequencies of the two maxima, which is typical for harmonics of different parity.

For this event, the ratios of *PSD* to the phase difference between $B_N$ and $B_E$ for the two satellites are different and depend greatly on frequency, thereby making a simple estimate of the source position impossible. This spatial distribution of amplitude and phase is probably related to the excitation of resonance and waveguide modes in the ionosphere.

For both events, disturbances begin almost synchronously, and high coherence is observed at the frequencies of the main spectral maxima. This allows us to interpret the observed magnetic field variations as pulsations. Their amplitude is much higher than that of the background magnetic field variations in the ionosphere, which does not exceed 0.1 nT. The vertical component amplitude (omitted in the figure) is more than an order of magnitude lower than that of the horizontal components, which corresponds to an Alfvén wave. In the former event, at a distance between the satellites, the oscillation spectra vary slightly; and in the latter, considerably. This suggests that the spatial scale of the oscillations in the former case is larger than the distance between the satellites; and in the latter, of the order of the distance between the satellites. Thus, the disturbances considered can be represented as a beam of Alfvén waves with a diameter of several tens to several hundreds of kilometers. Let us consider the passage of such a beam through the ionosphere for event 1.

## 3. FIELD SPATIAL STRUCTURE. MODEL

The wave field spatial structure can be estimated within the framework of a model of Alfvén wave beam passage through the ionosphere [Fedorov et al., 2018].

We consider the ionospheric parameters, using the IRI-2007 model [Bilitza, Reinisch, 2008)]. For event 1, vertical distributions of the amplitude of the three magnetic field components for two beam radii $\rho_0$ are illustrated in Figure 7. The distance from the beam center is $0.8\rho_0$, which is close to the position of the radial amplitude distribution maximum. The azimuthal magnetic field component $B_\phi$ prevails at ionospheric heights $h>150$ km; the radial component $B_\rho$, on Earth. Assuming that the beam center is between the satellites and considering that the satellites are located almost strictly along the geomagnetic meridian, we obtain that in the ionosphere $B_\phi$ approximately corresponds to the latitudinal component; and $B_\rho$, to the meridional one. At ionospheric heights, the amplitude oscillates with height with a spatial period of ~100 km, and positions of the extremes depend on the beam radius.

Radial distributions of magnetic field component amplitudes at the height of the satellite and on the Earth surface are shown in Figure 8. The maximum amplitude of the azimuthal component prevailing in the ionosphere

is at radial distances $(0.7\div0.8)\rho_0$. On the Earth surface, the vertical component prevails in a narrow region near the projection of the beam axis; the radial component, at distances larger than 30 km from the axis projection.

The main difference of the surface distribution from the ionospheric one is a weaker dependence of the magnetic field amplitude on the radial distance. Figure 9 depicts the dependence of the ratio $R_{GI}$ of the magnetic field amplitude on Earth to the maximum amplitude in the ionosphere on the distance to the beam center. The position of the maximum and the maximum value of $R_{GI}$ depend on the beam radius $\rho_0$. The ratio of the distance between the beam center and $\rho_{max}$ to $\rho_0$ increases, and $R_{GI}$ at a maximum decreases with decreasing beam radius ($\rho_{max}/\rho_0=1$ and $R_{GI}=6\cdot10^{-2}$ at $\rho_0=100$ km, and at $\rho_0=25$ km $\rho_{max}/\rho_0=2$ and $R_{GI}=5\cdot10^{-3}$). Thus, supposing that the pulsations detected in event 1 occurred near the maximum of the radial amplitude distribution in the ionosphere, we obtain a lower-bound estimate for the amplitude on the Earth surface. Depending on the beam radius, it can
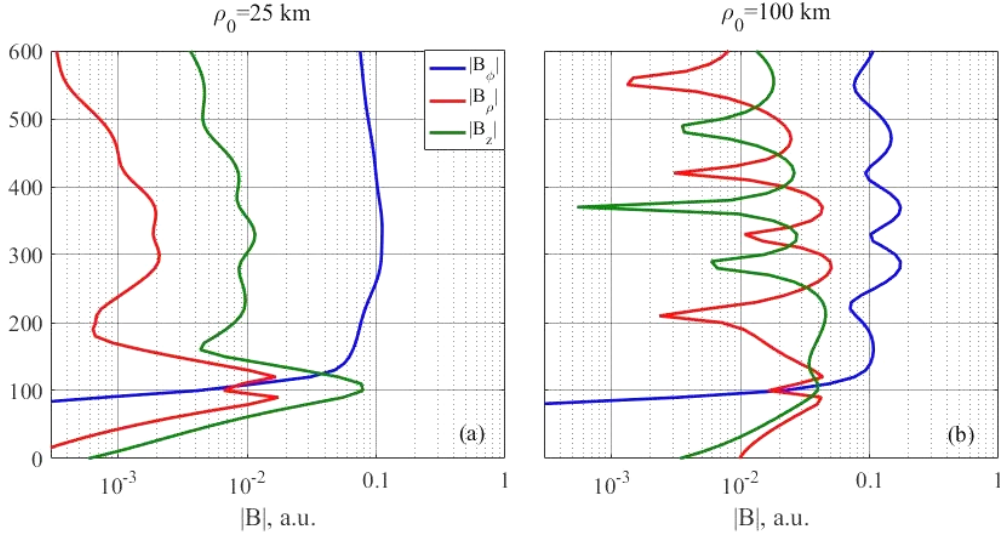


*Figure 7*. Vertical distribution of magnetic field component amplitudes for an Alfvén beam of finite radius $\rho_0$ incident on the ionosphere for a frequency of 4 Hz. Ionospheric conditions correspond to event 1
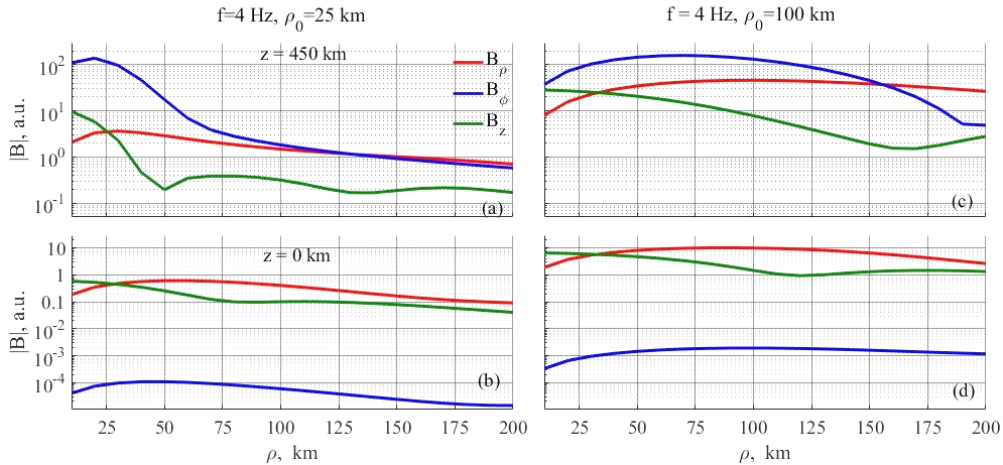


*Figure 8*. Radial distribution of magnetic field component amplitudes at a satellite height (top panels) and on the Earth surface (bottom panels) for the same geometry of incident wave beam and frequency as in Figure 7
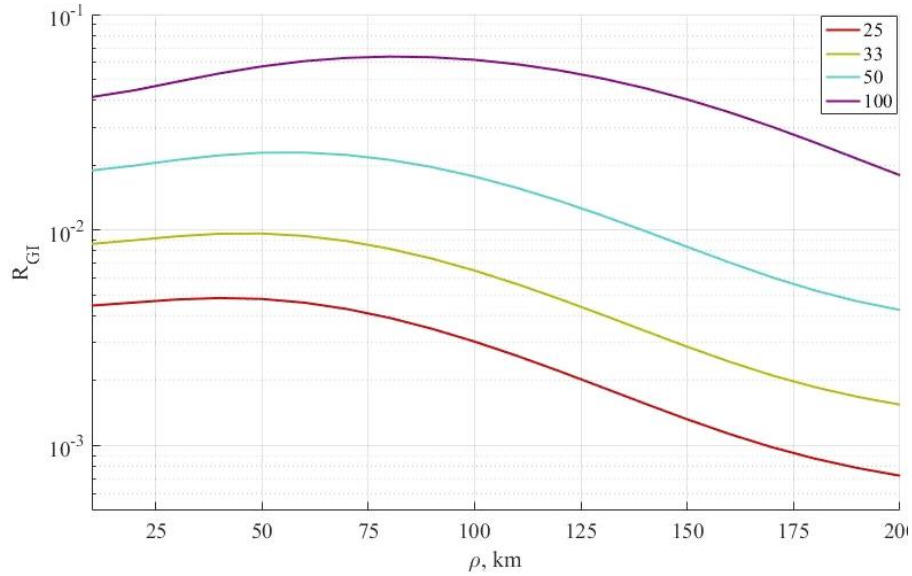
*Figure 9.* Radial distribution of the ratio $R_{GI}$ of the magnetic field amplitude on the Earth surface to the maximum amplitude at a satellite height as a function of wave beam radius for a frequency of 4 Hz under the same ionospheric conditions as in Figures 7, 8

it can range from several hundredths to several tenths of nT. In the latter case, these pulsations can be detected on Earth even with a flux gate magnetometer at a distance to 200 km from the beam center projection.

## 4. DISCUSSION

The signals considered can have both magnetospheric and atmospheric origin associated with penetration of the Schumann resonance into the ionosphere [Ni, Zhao, 2005; Surkov et al., 2013]. Until the present, experimental evidence for the penetration of the Schumann resonance to ionospheric heights has been observed only for the electrical component, although the weak maxima in Figure 1 detected at low and middle latitudes can have an atmospheric origin. A possible source of such signals can be individual slow discharges caused by an upward current with a charge moment of the order of or greater than 100 C·km [Rakov, Uman, 2003]. Theoretical analysis of the field structure from an atmospheric discharge with a charge moment of $10^3$ C·km under nighttime ionospheric conditions [Mazur et al., 2018] has shown that the field from the discharge slowly (as $1/\rho$) decreases with horizontal distance, which makes it possible to detect a signal with an amplitude above 1 nT at distances of the order of $10^3$ km from a point above the lightning discharge. At distances to 400 km, positions of spectral maxima are determined by IAR; at longer distances, the spectrum is mainly defined by the waveguide mode, and maxima appear in it at frequencies above 4 Hz. Discharges with a charge moment above 100 C·km account for several percent of all recorded lightnings, and their occurrence decreases with increasing intensity, so that the discharges with a charge moment of the order of or greater than $10^3$ C·km are rare events for which the presence of ionospheric disturbances can be directly monitored. What might argue for the atmospheric origin of the maxima observed at low and middle latitudes is their coincidence in time with

discharges of extreme intensity, as well as spectra consistent with the calculated ones. The spatial distribution can be analyzed using SWARM data only for individual events for which the distance between satellites A/C and B is $10^2$–$10^3$ km.

For the high-latitude oscillations under study, the magnetospheric source seems to be the most likely. This hypothesis is supported by the coincidence of the zones of the highest oscillation power with the latitudes of ionospheric projections of the polar cusp/cleft and magnetospheric input layers. In these regions, the main magnetic field in the magnetosphere is highly nonuniform in strength and direction, which can lead to unstable particle distributions, including temperature anisotropy. Transverse proton temperature anisotropy is a condition for the excitation of ion-cyclotron oscillations [Sagdeev, Shafranov, 1960]. In the inner magnetosphere, the generation region of ion-cyclotron waves lies near the equator at distances no greater than 11° [Loto'aniu et al., 2005], and their frequencies fall within the Pc1 range. The ionospheric oscillations of higher frequencies we have examined generally occur at latitudes near and above the auroral oval polar boundary, and their frequencies correspond to the frequencies of proton-cyclotron resonance for the magnetic field **B** of the order of hundreds of nT. For the polar cusp/cleft, mantle, and magnetospheric input layers, **B** corresponds to intermediate magnetic latitudes (30–60° from the equatorial plane of the magnetosphere).Intense oscillations with frequencies from fractions of hertz to several hertz outside the equatorial region of the magnetosphere in the field lines corresponding to cusp/cleft projections were recorded by the POLAR satellite [Le et al., 2011]. This is due to the fact that the region of ion-cyclotron wave generation is linked to the region of the minimum absolute magnetic field, which is shifted from the equator in the vicinity of the polar cusp/cleft and in the magnetospheric input layers [Shabansky, 1971]. The statistical distribution of occurrence of ion-cyclotron waves

in the magnetosphere in the Pc1–2 frequency range indicates that they are generally recorded in the daytime sector for $L>8$ (see [Usanova et al., 2012] and references therein). This possibility has been explored theoretically in [McCollough et al., 2010, 2012]. A magnetic storm [Blum et al., 2009] or an abrupt change in the solar wind dynamic pressure [McCollough et al., 2010] is considered as external causes of unstable ion populations.

Vines et al. [2019] give experimental evidence of a source of ion-cyclotron waves remote from the equator (at a magnetic latitude of ~25°) in the afternoon sector of the outer magnetosphere. Simultaneous observations of the electromagnetic field and ion distributions made it possible to localize the source of the oscillations and establish that the observed ion distributions correspond to the distributions necessary for the excitation of ion-cyclotron waves. At the same time, the conditions outside the magnetosphere and the geomagnetic activity indices pointed to a weak disturbance. Thus, Vines et al. [2019] have demonstrated that there may be unstable ion distributions in the outer magnetosphere and associated ion-cyclotron waves without strong disturbances, which is indirectly confirmed by the results of our work.

Occurrence of EMIC waves in the outer magnetosphere at large distances from the equator was recorded by Cluster satellites [Rème et al., 2001], whose orbit covered the interval of $L$ shells from 4 $R_E$ to 20 $R_E$ and geomagnetic latitudes from 0° to 45°. Statistical analysis of occurrence of EMIC waves in the magnetosphere for ten years (2001–2010) has shown [Allen et al., 2015] that in the daytime sector (9–15 MLT), the maximum occurrence of waves in the outer magnetosphere $L>8$ falls within geomagnetic latitudes 15°–30° and exceeds 10 %; and at a distance 30°–45° from the equator, it decreases to several percent. Meanwhile, in the dusk sector (15–21 MLT), even for $L>14$ for magnetic latitudes 30°–45°, the average occurrence is several percent, running to 10 % for individual sectors. The dependence of the occurrence of magnetospheric EMIC-waves on $L$ and MLT according to [Allen et al., 2015] is qualitatively consistent with those shown in Figure 2 and PSD of the ionospheric oscillations studied in this work. Parameters of cold plasma and hot protons with energies from 10 to 40 keV for the same observation period have been analyzed in [Allen et al., 2016]. In the outer magnetosphere, for all magnetic latitudes at which EMIC waves were observed, higher levels of transverse temperature anisotropy and ratio β of hot proton pressure to the magnetic pressure have been found, with maximum β at the magnetic latitude of ~45°. The high-latitude ionospheric oscillations in the range of several hertz we have studied are most likely to be a manifestation of magnetospheric EMIC waves generated by anisotropic proton distributions in extra-equatorial regions of the outer magnetosphere [Allen et al., 2015, 2016].

Another source of the ionospheric oscillations in the range above the nominal Pc1 is lower-frequency magnetospheric EMIC waves generated at shorter distances from the equator. Liu et al. [2019] reported Pc1 pulsations recorded simultaneously by four MMS satellites in the outer magnetosphere at approximately the same distance from the equator as in [Vines et al., 2019]. The distance between the satellites in the magnetosphere

was 50–100 km, the meridional distance between the ionospheric projections, 0.02°, i.e. ~2 km. Dynamic spectra of the pulsations were similar, but not identical for all MMS satellites, and the differences were noticeable even in the figures given in the article, where the total time was 90 min. Thus, the Pc1 pulsations of magnetospheric origin, which have kilometer transverse scales at the ionospheric height, can contribute to the higher-frequency magnetic field variations in the ionosphere recorded by low-orbit satellites.

The analysis of coherent ionospheric oscillations we have carried out using a time window of 2.56 s allows us to separate the temporal and spatial field variations on the time scales of the order of or greater than 10 s, and the amplitude threshold used makes it possible to classify wave packets observed simultaneously by two satellites with a duration of several periods, similar to those shown in Figures 5, 6, as oscillations whose spectra vary slightly when measured by a low-orbit satellite and a stationary sensor. The intermediate frequency range from fractions to a few of hertz, kilometer spatial scales, and wave packet durations from 3 to 10 s requires special analysis methods to separate spatial and temporal variations.

## CONCLUSIONS

1. Geomagnetic variations at frequencies 2.5–12 Hz in the ionospheric F layer above the maximum electron density recorded by SWARM satellites exhibit the maximum occurrence and amplitude at latitudes near and above the auroral oval polar boundary corresponding to the regions of magnetospheric input layers and dayside polar cusp/cleft.

2. The high coherence of variations for two spaced satellites makes it possible to identify them as wave disturbances with a scale larger than the distance between the satellites.

3. A possible source of these disturbances is ion-cyclotron waves in the extra-equatorial regions of the outer magnetosphere.

## REFERENCES

Allen R.C., Zhang J.-C., Kistler L.M., Spence H.E., Lin R.-L., Klecker B., et al. A statistical study of EMIC waves observed by Cluster: 1. Wave properties. *J. Geophys. Res.: Space Phys.* 2015, vol. 120, pp. 5574–5592. DOI: 10.1002/2015JA021333.

Allen R.C., Zhang J.-C., Kistler L.M., Spence H.E., Lin R.-L., Klecker B., et al. A statistical study of EMIC waves observed by Cluster: 2. Associated plasma conditions. *J. Geophys. Res.: Space Phys.* 2016, vol. 121, pp. 6458–6479. DOI: 10.1002/2016JA022541.

Arnoldy R.L., Engebretson M.J., Denton R.E., Posch J.L., Lessard M.R., Maynard N.C., et al. Pc1 waves and associated unstable distributions of magnetospheric protons observed during a solar wind pressure pulse. *J. Geophys. Res.* 2005, vol. 110, A07229. DOI: 10.1029/2005JA011041.

Belyaev P.P., Bosinger T., Isaev S.V., Trakhtengerts V.Y., Kangas J. First evidence at high latitude for the ionospheric Alfvén resonator. *J. Geophys. Res.* 1999, vol. 104, pp. 4305–4318.

Bilitza D., Reinisch B. International Reference Ionosphere. Improvements and new parameters. *Adv. Space Res.* 2008, vol. 42, pp. 599–609. DOI: 10.1016/j.asr.2007.07.048.

Blum L.W., MacDonald E.A., Gary S.P., Thomsen M.F., Spence H.E. Ion observations from geosynchronous orbit as a proxy for ion cyclotron wave growth during storm times. *J. Geophys. Res.* 2009, vol. 114, A10214. DOI: 10.1029/2009JA014396.

Bogdanova Y.V., Fazakerley A.N., Owen C.J., Klecker B., Cornilleau-Wehrlin N., Grison B., et al. Correlation between suprathermal electron bursts, broadband extremely low frequency waves, and local ion heating in the midaltitude cleft/low-latitude boundary layer observed by Cluster. *J. Geophys. Res.* 2004, vol. 109, A12226. DOI: 10.1029/2004JA010554.

Buchsbaum S.J. Ion resonance in a multicomponent plasma. *Phys. Rev. Lett.* 1960, vol. 5, no. 11, pp. 495–497. DOI: 10.1103/PhysRevLett.5.495.

Engebretson M.J., Onsager T.G., Rowland D.E., Denton R.E., Posch J.L., Russell C.T., et al. On the source of Pc1-2 waves in the plasma mantle. *J. Geophys. Res.* 2005, vol. 110, A06201. DOI: 10.1029/2004JA010515.

Engebretson M.J., Posch J.L., Westerman A.M., Otto N.J., Slavin J.A., Le G., et al. Temporal and spatial characteristics of Pc1 waves observed by ST5. *J. Geophys. Res.* 2008, vol. 113, A07206. DOI: 10.1029/2008 JA013145.

Ermakova E.N., Yakhnin A.G., Yakhnina T.A., Demekhov A.G., Kotik D.S. Sporadic geomagnetic pulsations at frequencies up to15 Hz in the magnetic storm of November 7–14, 2004: features of the amplitude and polarization spectra and their connection with ion-cyclotron wave in the magnetooshhere. Radiophys Quantum El. 2016, vol. 58, pp. 547–560. DOI: 10.1007/s11141-016-9628-3.

Fedorov E.N., Pilipenko V.A., Engebretson M.J., Hartinger M.D. Transmission of a magnetospheric Pc1 wave beam through the ionosphere to the ground. *J. Geophys. Res.: Space Phys.* 2018, vol. 123, pp. 3965–3982.DOI: 10.1029/2018JA025338.

Feldstein Y.I. On Morphology and Auroral and Magnetic Disturbances at High Latitudes. *Geomagnetism and Aeronomy.* 1963, vol. 3, p. 138.

Francia P., Regi M., de Lauretis M., Pezzopane M., Cesaroni C., Spogli L., Raita T. A case study of correspondence between Pc1 activity and ionospheric irregularities at polar latitudes. *Earth Planets Space.* 2020, vol. 72, 59. DOI: 10.1186/s40623-020-01184-4.

Guglielmi A.V., Potapov A.S., Dovbnya B.V. On the origin of frequency modulation of serpentine emission. *Solar-Terr. Phys.* 2015, vol. 1, pp. 85–90.

Holzworth R.H., Meng C.-I. Mathematical representation of the auroral oval. *Geophys. Res. Lett.* 1975, vol. 2, pp. 377–380.DOI: 10.1029/GL002i009p00377.

Jacobsen K.S., Moen J.I. On the correlation between broad-band ELF wave power and ion fluxes in the cusp. *Ann. Geophys.* 2010, vol. 28, pp. 1249–1261. DOI: 10.5194/angeo-28-1249-2010.

Jenkins G., Watts D. Spectral analysis and its applications, Holden-Day, San Francisco, London, Amsterdam, 1969, 525 p.

Juusola L., Kauristie K., Vanhamäki H., Aikio A., van de Kamp M. Comparison of auroral ionospheric and field-aligned currents derived from Swarm and ground magnetic field measurements. *J. Geophys. Res.: Space Phys.* 2016, vol. 121, pp. 9256–9283. DOI: 10.1002/2016JA022961.

Kataoka R., Fukunishi H., Lanzerotti L.J. Statistical identification of solar wind origins of magnetic impulse events. *J. Geophys. Res.* 2003, vol. 108, iss. A12, p. 1436. DOI: 10.1029/ 2003JA010202.

Kim H., Lessard M.R., Engebretson M.J., Young M.A. Statistical study of Pc1–2 wave propagation characteristics in the high-latitude ionospheric waveguide. *J. Geophys. Res.* 2011, vol. 116, A07227. DOI: 10.1029/2010JA016355.

Kim H., Shiokawa K., Park J., Miyoshi Y., Stolle C., Buchert S. Statistical analysis of Pc1 wave ducting deduced from Swarm satellites. *J. Geophys. Res.: Space Phys.* 2021, vol. 126, e2020JA029016. DOI: 10.1029/2020JA029016.

Lanzerotti L.J., Konik R.M., Wolfe A., Venkatesan D., Maclennan C.G. Cusp latitude magnetic impulse events, 1, Occurrence statistics. *J. Geophys. Res.* 1991, vol. 96, pp. 14009–14022.

Le Queau D., Roux A. Heating of Oxygen Ions by Resonant Absorption of Alfvén Waves in a Multicomponent Plasma. *J. Geophys. Res.* 1992, vol. 97, pp. 14929–14946. DOI: 10.1029/92JA01052.

Le G., Chi P.J., Strangeway R.J., Slavin J.A. Observations of a unique type of ULF wave by low-altitude Space Technology 5 satellites. *J. Geophys. Res.* 2011, vol. 116, iss. A08. DOI: 10.1029/2011JA016574.

Leonovich A.S., Mazur V.A., Senatorov V.N. Alfvén waveguide. Zh. Eksp. Teor. Fiz. 1983, vol. 85, pp. 141–145.

Liu S., Xia Z., Chen L., Liu Y., Liao Z., Zhu H. Magnetospheric Multiscale Observation of quasiperiodic EMIC waves associated with enhanced solar wind pressure. *Geophys. Res. Lett.* 2019, vol. 46, pp. 7096–7104. DOI: 10.1029/2019GL083421.

Loto'aniu T.M., Fraser B.J., Waters C.L. Propagation of electromagnetic ion cyclotron wave energy in the magnetosphere. *J. Geophys. Res.* 2005, vol. 110, iss. A07. DOI: 10.1029/ 2004JA010816.

Lühr H., Park J., Gjerloev J.W., Rauberg J., Michaelis I.G. Merayo J.M., Brauer P. Field-aligned currents' scale analysis performed with the Swarm constellation. *Geophys. Res. Lett.* 2015, vol. 42, pp. 1–8. DOI: 10.1002/2014GL062453.

Mazur N.G., Fedorov E., Pilipenko V.A., Vakhnina V. ULF electromagnetic field in the upper ionosphere excited by lightning. *J. Geophys. Res.: Space Phys.* 2018, vol. 123, pp. 6692–6702. DOI: 10.1029/2018JA025622.

McCollough J.P., Elkington S.R., Usanova M.E., Mann I.R., Baker D.N., Kale Z.C. Physical mechanisms of compressional EMIC wave growth. *J. Geophys. Res.* 2010, vol. 115, A10214, DOI: 10.1029/2010JA015393.

McCollough J.P., Elkington S.R., Baker D.N. The role of Shabansky orbits in compression-related electromagnetic ion cyclotron wave growth. *J. Geophys. Res.* 2012, vol. 117, A01208. DOI: 10.1029/2011JA016948.

Mikhailova O.S., Klimushkin D.Yu., Mager P.N. The current state of the theory of Pc1 range ULF pulsations in magnetospheric plasma with heavy ions: a review. Solar-Terrestrial Physics. 2022, vol. 8, iss. 1, pp. 3–18.

Newell P.T., Sotirelis T., Ruohoniemi J.M., Carbary J.F., Liou K., Skura J.P., et al. OVATION: Oval variation, assessment, tracking, intensity, and online nowcasting. *Ann. Geophys.* 2002, vol. 20, pp. 1039–1047. DOI: 10.5194/angeo-20-1039-2002.

Newell P.T., Sotirelis T., Liou K., Lee A.R., Wing S., Green J., Redmon R. Predictive ability of four auroral precipitation models as evaluated using Polar UVI global images. *Space Weather.* 2010, vol. 8, S12004. DOI: 10.1029/ 2010SW000604.

Ni B.-B., Zhao Z.-Yu. Spatial observations of Schumann resonance at the ionospheric altitude. *Chinese Journal of Geophysics*. 2005, vol. 48, pp. 818–826.

Nykyri K., Grison B., Cargill P.J., Lavraud B., Lucek E., Dandouras I., et al. Origin of the turbulent spectra in the high-altitude cusp: Cluster spacecraft observations. *Ann. Geophys*. 2006, vol. 24, pp. 1057–1075. DOI: 10.5194/angeo-24-1057-2006.

Olsen N., Friis-Christensen E., Floberghagen R., Alken P., Beggan C.D., Chulliat A., et al. The Swarm satellite constellation application and research facility (SCARF) and Swarm data products. *Earth Planets Space*. 2013, vol. 64, P. 1189–1200. DOI: 10.5047/eps.2013.07.001.

Papitashvili V.O., Papitashvili N.E., King J.H. Magnetospheric geomagnetic coordinates for space physics data presentation and visualization. *Adv. Space Res*. 1997, vol. 20, pp. 1097–1100. DOI: 10.1016/S0273-1177(97)00565-6.

Parkhomov V.A., Zastenker G.N., Riazantseva M.O., Tsegmed B., Popova T.A. Bursts of geomagnetic pulsations in the frequency range 0.2–5 Hz excited by large changes of the solar wind pressure. *Cosmic Res*. 2010, vol. 48, pp. 86–100. DOI: 10.1134/S0010952510010077.

Parkhomov V.A., Dovbnya B.V., Borodkova N.A., Safargaleyev V.V., Pashinin A.Yu. Pulse bursts of geomagnetic pulsations in the frequency range of 0.2–7 Hz as a first signal of interaction between interplanetary shock waves and the magnetosphere. Solar-Terrestrial Physics. 2014, no. 25(138), pp. 21–28. (In Russian).

Pilipenko V.A., Polozova T.L., Engebretson M. Space-time structure of ion-cyclotron waves in the topside ionosphere as observed onboard the ST-5 satellites. *Cosmic Res*. 2012, vol. 50, pp. 329–339. DOI: 10.1134/S0010952512050048.

Polyakov S.V., Rapoport V.O. Ionospheric Alfvén resonator. *Geomagnetism and Aeronomy*. 1981, vol. 21, pp. 816–822.

Rakov V.A., Uman M.A. Lightning: Physics and Effects. Cambridge U. Press, New York, 2003, 687 p.

Rème H., Aoustin C., Bosqued J.M., Dandouras I., Lavraud B., Sauvaud J.A., Barthe A., Bouyssou J., Camus Th., et al. First multispacecraft ion measurements in and near the Earth's magnetosphere with the identical Cluster ion spectrometry (CIS) experiment. *Ann. Geophys*. 2001, vol. 19, iss.10-12, pp. 1303–1354. DOI: 10.5194/angeo-19-1303-2001.

Sagdeev R.Z., Shafranov V.D. On the instability of the plasma with an anisotropic distribution of velocities in a magnetic field. Soviet Phys. JETP. 1961, vol. 12, pp. 130–132.

Sato M., Fukunishi H., Lanzerotti L.J., Maclennan C.G. Magnetic impulse events and related Pc1 bursts observed by the Automatic Geophysical Observatories network in Antarctica. *J. Geophys. Res*. 1999, vol. 104, pp. 19971–19982. DOI: 10.1029/1999JA900111.

Shabansky V.P. Some processes in the magnetosphere. *Space Sci. Rev*. 1971, vol. 12, P. 299–418. DOI: 10.1007/BF00165511.

Simões F., Pfaff R.F., Freudenreich H. Observation of Schumann resonances in the Earth's ionosphere. *Geophys. Res. Lett*. 2011, vol. 38, L22101. DOI: 10.1029/2011GL049668.

Slavin J.A., Le G., Strangeway R.J., Wang Y., Boardsen S.A., Moldwin M.B., E. Spence H. Space Technology 5 multi-point measurements of near-Earth magnetic fields: Initial results. *Geophys. Res. Lett*. 2008, vol. 35, L02107. DOI: 10.1029/2007GL031728.

Surkov V.V., Nosikova N.S., Plyasov A.A., Pilipenko V.A., Ignatov V.N. Penetration of Schumann resonances into the upper ionosphere. *J Atmos. Solar-Terr. Phys*. 2013, vol. 97, pp. 65–74. DOI: 10.1016/j.jastp.2013.02.015.

Usanova M.E., Mann I.R., Bortnik J., Shao L., Angelopoulos V. THEMIS observations of electromagnetic ion cyclotron wave occurrence: Dependence on *AE*, *SYM-H*, and solar wind dynamic pressure. *J. Geophys. Res*. 2012, vol. 117, A10218. DOI: 10.1029/2012JA018049.

Vines S.K., Allen R.C., Anderson B.J., Engebretson M.J., Fuselier S.A., Russell C.T., et al. EMIC waves in the outer magnetosphere: Observations of an offequator source region. *Geophys. Res. Lett*. 2019, vol. 46, pp. 5707–5716. DOI: 10.1029/2019GL082152.

URL: https://swarm-diss.eo.esa.int (accessed November 16, 2022).

URL: https://cdaweb.gsfc.nasa.gov (accessed November 16, 2022).